

# Distributed Multi-Pole Model for Motion Simulation of PM-based Spherical Motors

Hungsun Son and Kok-Meng Lee\*, *Fellow, IEEE*

**Abstract**— Design and control of multi degrees of freedom (DOF) electromagnetic actuators require a good understanding of the magnetic fields, and involve real-time calculation of magnetic forces. This paper presents a new method to derive closed-form solutions for characterizing the magnetic field of permanent magnets (PM), and their uses in modeling the magnetic torque of a PM-based spherical motor. The method, referred here as distributed multi-pole (DMP) model, inherits many advantages of the dipole model originally conceptualized in the context of physics, but provides an effective means to account for the shape and magnetization of the physical magnet. The DMP models have been validated by comparing the calculated fields and magnetic forces against numerical and experimental results. The comparisons show excellent agreement. We also illustrate the application of the DMP model in developing an accurate torque model to faithfully simulate the transient response of a spherical motor, and as a basis for deriving a closed-form inverse torque model for its real-time current optimization. While developed in the context of a spherical motor, the modeling techniques presented in this paper are applicable to other PM-based actuator and sensing systems.

## I. INTRODUCTION

Many meat handling and processing equipment, machine tools, mobile vehicles such as car wheels [1] [2], propellers for boats, helicopter or underwater vehicle, and gyroscopes require orientation control of a rotating shaft. The growing interests in fuel-cell technology and low-cost electric vehicles have motivated a number of researchers to develop application oriented in-wheel motors or multi-DOF spherical motors. In real-time control and analysis of a spherical motor, both the forward and inverse torque models are required.

Existing techniques for analyzing electromagnetic fields and real time of a multi-DOF PM-based actuator rely primarily on three approaches; namely, analytic solutions to Laplace equation, numerical methods and lumped-parameter analyses with some form of magnetic equivalent circuits [3]. The possibility of obtaining an analytic solution is often remote for devices with complex geometry. Perturbation theory and linear superposition can sometimes render a difficult problem solvable. However, even if an analytic solution is achievable, it often results in a series of space harmonics of non-elementary functions [4] [5] which have to

be computed if a numeric solution to the problem is desired. Numerical methods (such as finite element method) offer a good prediction of the magnetic field for accurate computation of the magnetic torque [6] [7]. However, demanding computational time limits these numerical methods to off-line computation. Most of the real-time computations for optimization and motion control of electromagnetic actuators have been relied on lumped parameter approaches in order to obtain a closed-form solution which generally yields only first-order accuracy. These approaches have difficulties in achieving both accuracy and low computation time simultaneously. Thus, we develop a new modeling method to derive closed-form field solutions for efficient design and motion control of the actuators.

An alternative method is based on the concept of a magnetic dipole (originally suggested by Fitz Gerlad in 1883) as a tool to characterize the magnetic potential fields. While the dipole model has been widely used to analyze the magnetic field at a sufficiently large distance for applications [8-10] such as electromagnetic wave propagation for antenna dynamics and geomagnetism to analyze earth polarization, it generally gives a poor approximation when the length scale of the field is very small. For reasons including compact formulation/solutions and intuitive magnetic fields, many researchers (for examples, [11] and [12]) continue to develop dipole models to analyze actuator designs involving permanent magnets. Nedelcu *et al.* [11] used a magnetic dipole model to describe the field of a PM-based device, where each PM is modeled as a doublet. While the model in [11] provides a concise computational formulae for the field and the energy flow, it has difficulties to obtain an accurate magnetic field. Visschere [12] later pointed out a number of mistakes by comparing the dipole approximation in [9] against an analytical 2D magnetic field solution of a PM. The existing single dipole model (equivalent to the mathematical theory of a doublet) is often studied in the context of physics and valid only for needle-like magnets; thus, it has very limited applications in modern actuator designs.

We present a general method, referred here as distributed multi-pole (DMP) model, for precise calculation of the magnetic field around a PM. This method inherits many advantages of the dipole model but provides an effective means to account for the shape and magnetization of the physical PM. The remainder of this paper offers the following:

1. We present the DMP model that uses a limited set of

Manuscript received on June 30, 2007. This work was supported by the Georgia Agricultural Technology Research Program (ATRP) and the U. S. Poultry and Eggs Association. The authors are with the Woodruff School of Mechanical Engineering, Georgia Institute of Technology  
\* Corresponding author: [kokmeng.lee@me.gatech.edu](mailto:kokmeng.lee@me.gatech.edu); tel: +1(404)894-7402; fax: +1(404)894-9342.

known field points to construct an analytical model consisting of multiple dipoles to obtain the closed-form field solutions around a PM. The simplicity of the DMP model offers an advantage for real-time applications.

2. We illustrate the procedure of developing a DMP model for characterizing the magnetic field of a spherical motor, which consists of cylindrical PM's and multi-layer electromagnets EM. The DMP models are validated by comparing the simulated fields and calculated magnetic forces against known solutions whenever possible, and/or published numerical simulations and experimental results. The comparisons show excellent agreement.
3. We also illustrate how the DMP model can be used to develop the forward and inverse torque models for motion control of a spherical motor. The forward model computes the torque and along with the solutions to the rotor dynamics, simulates the rotor motion. The inverse model that computes an optimized set of currents to provide the desired torque for tracking the desired trajectory, however, must be controlled in real time. As will be shown, the DMP model presented here provides a means to derive a closed-form inverse torque model for real-time current optimization while retain the full torque model to faithfully predict the motion of the spherical motor.

## II. CLOSED-FORM FIELD MODELING METHOD

Design of electromagnetic actuators and their control involves calculation of magnetic forces. The Lorenz force equation is commonly used to calculate the magnetic force exerted on current-carry conductors:

$$\mathbf{F} = -\oint \mathbf{B} \times I d\boldsymbol{\ell} \quad \text{where} \quad I = -\oint \mathbf{J} \cdot d\mathbf{S} \quad (1)$$

where  $\boldsymbol{\ell}$  is the normalized current direction vector. In (1), the current density vector  $\mathbf{J}$  is directly used in the calculation and thus, it is not necessary to compute the magnetic flux generated by the current loop. Thus, the Lorenz force calculation involves only modeling the  $\mathbf{B}$ -fields of the PM's.

The solution to the force equation (1) requires solving the magnetic field. A method to model the magnetic field solutions in closed-form is to use multiple dipoles, which take into account the shape of the physical PM. Cylindrical PM are commonly used, and some analytical and experimental results are available for model validation; they are used here for clarity to illustrate the DMP modeling procedure. However, the method can be extended to PM of customized shape.

We consider here PM-based actuator applications which satisfy the following assumptions: the field is continuous and irrotational; and the medium is homogeneous. The irrotational field  $\nabla \times \mathbf{B} = 0$  enables us to define a scalar magnetic potential  $\Phi$  such that the magnetic field intensity  $\mathbf{H}$  is given by

$$\mathbf{H} = -\nabla \Phi \quad \text{and} \quad \mathbf{B} = \mu_0 \mathbf{H} \quad (2a,b)$$

where  $\mu_0$  is free space permeability. Since the field is continuous  $\nabla \cdot \mathbf{B} = 0$  and  $\mu_0$  is a constant, we have  $\nabla^2 \Phi = 0$ . The solution to Laplace's equation, which satisfies the field for a pole [10] which may be a source or a sink, is given by

$$\Phi = (-1)^j m / (4\pi R) \quad (3)$$

where  $m$  is the strength of the pole;  $j$  takes the value 0 or 1 designating that the pole is a source or a sink respectively; and  $R$  is the distance from the pole to the field point.

Since a single pole does not exist alone in a magnet filed, we define a *dipole* here as a pair of source and sink separated by a distance  $\bar{\ell}$ . An effective method to derive approximate flux paths of a magnet is to use multiple dipoles to account for the shape of the physical magnet. For design and control of PM-based devices, we seek the field solution outside the physical region of the magnets, particularly near its boundary.

Figure 1 shows the DMP model of the cylindrical magnet (radius  $a$ , length  $\ell$  and  $\mathbf{M} = M_o \mathbf{e}_z$ ), where  $k$  circular loops (each with radius  $\bar{a}_j$ ) of  $n$  dipoles are placed in parallel to the magnetization vector. The  $k$  loops are uniformly spaced:

$$\bar{a}_j = a j / (k + 1) \quad \text{at} \quad z = \pm \bar{\ell} / 2; \quad \text{where} \quad j = 0, 1, \dots, k \quad (4)$$

$$0 < \bar{\ell} < \ell \quad (5)$$

In Fig. 1,  $R_{ji+}$  and  $R_{ji-}$  are the distances from the  $i^{\text{th}}$  source and sink in  $j^{\text{th}}$  loop to any point  $P(x,y,z)$  respectively and given by

$$R_{ji\pm}^2 = [x - \bar{a}_j \cos i\theta]^2 + [y - \bar{a}_j \sin i\theta]^2 + (z \mp \bar{\ell} / 2)^2 \quad (6)$$

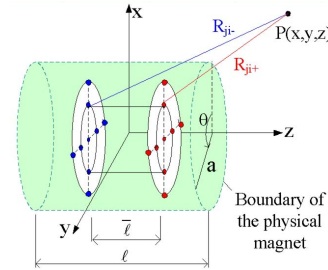


Fig. 1 DMP model of a cylindrical magnet

For a cylindrical magnet, the field is uniform circumferentially and thus, we set the dipole moment  $m_{ji} = m_j$ . To minimize the field variation in the  $\theta$  direction, we impose the following constraint on  $n$ :

$$\left. \frac{\text{Max}[\Phi(\theta)] - \text{Mean}[\Phi(\theta)]}{\text{Mean}[\Phi(\theta)]} \right|_{r=a, z=\ell/2} \times 100\% \leq \varepsilon_\theta \quad (7)$$

where  $\varepsilon_\theta$  is a specified (positive) error bound.

Since Laplace equation is linear, the magnetic field  $\Phi(x,y,z)$  of the PM can be obtained by summing the magnetic fields contributed by the individual poles:

$$\Phi = \frac{1}{4\pi} \sum_{j=0}^k m_j \sum_{i=1}^{n_k} \left( \frac{1}{R_{ji+}} - \frac{1}{R_{ji-}} \right) \quad \text{where} \quad n_k = \begin{cases} 1 & \text{if } j = 0 \\ n & \text{if } j \neq 0 \end{cases} \quad (8)$$

Similarly, the flux density at  $P$  can be found from (2):

$$\mathbf{B} = \frac{\mu_o}{4\pi} \sum_{j=0}^k m_j \sum_{i=1}^{n_k} \left( \frac{\mathbf{a}_{R_{ji+}}}{R_{ji+}^2} - \frac{\mathbf{a}_{R_{ji-}}}{R_{ji-}^2} \right) \quad \text{where} \quad n_k = \begin{cases} 1 & \text{if } j = 0 \\ n & \text{if } j \neq 0 \end{cases} \quad (9)$$

Since  $\nabla(1/R) = -\mathbf{a}_R(1/R^2)$  where  $\mathbf{a}_R (= \mathbf{R}/R)$ ,

$$\frac{\mathbf{a}_{R_{ji\pm}}}{R_{ji\pm}^2} = - \frac{(x - \bar{a}_j \cos i\theta) \mathbf{a}_x + (y - \bar{a}_j \sin i\theta) \mathbf{a}_y + (z \mp \bar{\ell} / 2) \mathbf{a}_z}{\left[ (x - \bar{a}_j \cos i\theta)^2 + (y - \bar{a}_j \sin i\theta)^2 + (z \mp \bar{\ell} / 2)^2 \right]^{3/2}}$$

The unknowns ( $k$ ,  $n$ ,  $\bar{\ell}$  and  $m_j$  where  $j = 0, \dots, k$ ) in the DMP model are solved by minimizing the error function (10)

subject to constraints imposed by the magnet geometry and a limited set of known field solutions (as fitting points):

$$E = \int_z [\Phi(z) - \Phi_A(z)]^2 dz \quad (10)$$

where  $\Phi_A(z)$  is the analytical solution along the magnetization axis. The general expression of  $\Phi_A$  from a magnetic pole at  $\mathbf{R}'(x', y', z')$  to the field point  $\mathbf{R}(x, y, z)$  is given in [11]:

$$\Phi_A(x, y, z) = \frac{1}{4\pi} \int_V \frac{-\nabla \cdot \mathbf{M}}{|\mathbf{R} - \mathbf{R}'|} dV + \frac{1}{4\pi} \int_S \frac{\mathbf{M} \cdot \mathbf{n}}{|\mathbf{R} - \mathbf{R}'|} dS$$

where  $\mathbf{n}$  is the unit surface normal; the first integral is a volume integral over the body volume  $V$  while the second is a surface integral over the body boundary surface  $S$ . In (10), the potential and flux density of a cylindrical PM along the  $z$ -axis can be expressed in closed form:

$$\frac{\Phi_A(Z)}{M_o \ell} = \frac{1}{4} [(A_- - |B_-|) - (A_+ - |B_+|)] \quad (11)$$

$$\frac{B_A(Z)}{\mu_o M_o} = \frac{1}{2} \left[ \frac{|B_+|}{A_+} - \frac{|B_-|}{A_-} + c \right] \quad \text{where} \quad (12)$$

$$c = \begin{cases} 0 & \text{if } |Z| \geq 1 \\ 2 & \text{if } |Z| < 1 \end{cases}$$

where  $Z = \frac{z}{\ell/2}$ ;  $\gamma = \frac{a}{\ell/2}$ ;  $A_{\pm} = \sqrt{\gamma^2 + B_{\pm}^2}$  and  $|B_{\pm}| = |Z \pm 1|$ .

For a given residual magnetic flux density, we have from (12):

$$\mathbf{B}(\ell/2) = \mathbf{B}_A(\ell/2) = -\mu_o \nabla \Phi_A|_{z=\ell/2} \quad (13)$$

where  $\mathbf{B}$  is given in (9). Since (10) accounts for the potential field along the magnetization axis, the remaining ( $k \times n + 1$ ) constraints are constructed from (8) and (9) along two other orthogonal directions. For PM-based actuator applications, the specified  $\Phi$  values are evaluated at an appropriate magnet surface. To avoid the singularity at  $\mathbf{R} = \mathbf{R}'$ , we choose

$$|R| = \lim_{\epsilon \rightarrow 0} \left( |R'| \Big|_{\text{point at surface}} + \epsilon_R \right)$$

where  $\epsilon_R$  is a small positive number. The procedure for modeling a PM is summarized as follows:

- 
- Step 1: Compute  $\Phi_A$  and  $\mathbf{B}_A$  analytically long the magnetization vector from (11) and (12) respectively
  - Step 2: Generate an initial set of spatial grid points ( $k, n$ ).
  - Step 3: Formulate (8) and (9) in terms of the unknowns,  $\bar{\ell}$  and  $m_{ji}$ .
  - Step 4: Find  $\bar{\ell}$  and  $m_{ji}$  by minimizing (10) subject to a set of constraints constructed from (11) and (12). Error computed by (9) is saved.
  - Step 5: Check if the condition (7) is satisfied. If yes, increase  $k$  or  $n$ , and repeat from Step 3. If no, the optimal parameters ( $k, n, \bar{\ell}$  and  $m_{ji}$ ) can be obtained by minimizing (10) using Step 4.
- 

### III. DMP-BASED TORQUE MODEL OF A SPHERICAL MOTOR

Figure 2 shows a CAD model of a spherical wheel motor (SWM) [14] based on a modified design of variable-reluctance spherical motors (VRSM) [6]. Unlike a VRSM where the rotor PM and stator EM poles are placed on locations following the vertices of a regular polygon, the PM's and EM's of a SWM are equally spaced on layers of circular planes such that their magnetization axes pass radially through the motor center.

#### A. Design Configuration of a Spherical Motor

The rotor PM's and stator EM's are grouped in pairs; every two pole-pairs form a plane providing a well-balanced symmetry electromechanically. In rotor coordinates ( $x, y, z$ ), the magnetization axes of the  $m_r$  rotor PM pairs are given by

$$\mathbf{r}_i = (-1)^{i-1} [\cos \phi_r \cos \theta_{ri} \quad \cos \phi_r \sin \theta_{ri} \quad \sin \phi_r]^T \quad (14)$$

where  $i = 1, 2, \dots, m_r$ ; and  $\theta_{ri} = (i-1)\theta_r$ . Similarly, the  $m_s$  stator EM pairs in the stator frame ( $XYZ$ ) are given by (15):

$$\mathbf{s}_j = [\cos \phi_s \cos \theta_{sj} \quad \cos \phi_s \sin \theta_{sj} \quad \sin \phi_s]^T \quad (15)$$

where  $j = 1, 2, \dots, m_s$ ; and  $\theta_{sj} = (j-1)\theta_s$ . Unlike  $m_s$  which may be odd or even,  $m_r$  is always an even number.

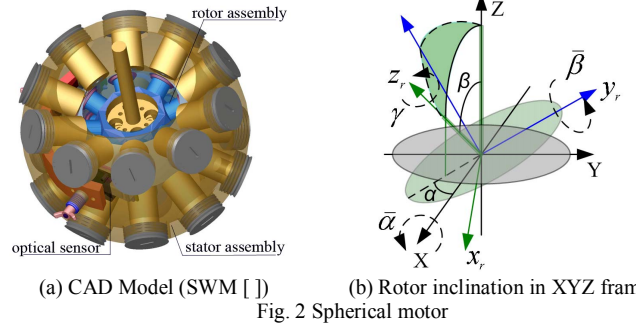


Fig. 2 Spherical motor

The inclination of a continuously spinning rotor is commonly described in terms of  $zyz$  Euler angles ( $\alpha, \beta, \gamma$ ) as it can be easily visualized as shown in Fig. 2(b). This representation, however, has singularities at  $\alpha = 0, \pm\pi$  which makes it difficult to compute numerically. Thus, the  $xyz$  Euler angles ( $\bar{\alpha}, \bar{\beta}, \gamma$ ) are used for the numerical computation of coordinate transformation:

$$\bar{\alpha} = -\sin^{-1}(\sin \alpha \sin \beta) \quad \text{and} \quad \bar{\beta} = \sin^{-1}(\sin \alpha \cos \beta / \cos \bar{\alpha}) \quad (16a, b)$$

To facilitate calculating the torque of the spherical motor in stator (inertia) frame, we define the transformation:

$$\mathbf{x}_s = \mathbf{L}_{sr} \mathbf{L}_{ri} \mathbf{x}_{ri} \quad (17)$$

where  $\mathbf{x}_{ri}$  the local coordinate frames of the  $i^{\text{th}}$  PM defined in Fig. 1;  $\mathbf{L}_{ri}$  describes the transformation from  $\mathbf{x}_{ri}$  to  $\mathbf{x}_r$ ,

$$\mathbf{L}_{ri} = \begin{pmatrix} \cos \phi_r & \sin \theta_{ri} \sin \phi_r & -\cos \theta_{ri} \sin \phi_r \\ -\sin \phi_r & \sin \theta_{ri} \cos \phi_r & -\cos \theta_{ri} \cos \phi_r \\ 0 & \cos \theta_{ri} & \sin \theta_{ri} \end{pmatrix};$$

and  $\mathbf{L}_{sr}$  from  $\mathbf{x}_r$  to  $\mathbf{x}_s$

$$\mathbf{L}_{sr} = \begin{pmatrix} \cos \phi_s \cos \bar{\beta} & \cos \phi_s \sin \bar{\alpha} \sin \bar{\beta} & -\cos \phi_s \cos \bar{\alpha} \sin \bar{\beta} + \sin \phi_s \sin \bar{\alpha} \\ -\sin \phi_s \cos \bar{\beta} & \cos \bar{\alpha} \cos \phi_s - \sin \phi_s \sin \bar{\alpha} \sin \bar{\beta} & \sin \phi_s \cos \bar{\alpha} \sin \bar{\beta} + \cos \phi_s \sin \bar{\alpha} \\ \sin \bar{\beta} & -\sin \bar{\alpha} \cos \bar{\beta} & \cos \bar{\alpha} \cos \bar{\beta} \end{pmatrix}$$

For a structure with linear magnetic properties, the magnetic field of the spherical motor is obtained from (8) summing over the DMP models of the rotor PM's with the coordinate transformation (17).

#### B. Torque Calculation

The resultant torque of the spherical motor has the form:

$$\mathbf{T} = [T_x \quad T_y \quad T_z]^T = [\mathbf{K}] \mathbf{u} \quad (18)$$

where  $\mathbf{K} (\in \mathbb{R}^{3 \times m_s}) = [K_1 \quad \dots \quad K_j \quad \dots \quad K_{m_s}]$ ; (18a)

$$\text{and } \mathbf{u} = [J_1 \cdots J_j \cdots J_{m_s}]^T \quad (18b)$$

In (18a),  $K_j \in \mathbb{R}^{3 \times 1}$  is the torque characteristic vector contributed by the  $j^{\text{th}}$  EM. In terms of rotor orientation,

$$K_j = \mathbf{L}_{s_j} \left( \oint_{EM} \mathbf{R} \times (\mathbf{J}_j / |\mathbf{J}_j|) \times \left[ \sum_{i=1}^{2m_r} \mathbf{B}_i(\alpha, \beta, \phi) \right] r dr d\theta d\ell \right) \quad (19)$$

where  $\mathbf{B}_i \in \mathbb{R}^{3 \times 1}$  is the flux density of the  $i^{\text{th}}$  PM;  $\mathbf{R}$  and  $r$  are the position vector and the radius of current conductor respectively; and  $\mathbf{L}_{s_j}$  is the coordinate transformation from  $\mathbf{x}_{s_j}$  (the local coordinate frame of the  $j^{\text{th}}$  EM) to  $\mathbf{x}_s$ , which has the same form as  $\mathbf{L}_{r_i}$  but replacing the angles in (15).

### C. Control System Analysis

For control and motion simulation of a spherical motor, both the forward and inverse torque models are required as illustrated in Fig. 3. For a given set of current inputs, the forward model (18) computes the torque and, along with the solutions to the equation of rotor dynamics given in the appendix, simulates the rotor motion. The inverse model that computes an optimized set of currents providing the necessary torque  $\mathbf{T}_d$  to track the desired trajectory  $\mathbf{x}_d$ , however, must be controlled in real time.

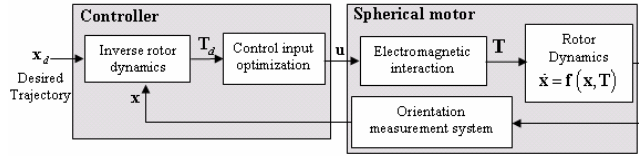


Fig. 3 Closed-loop control of the spherical motor

The torque characteristic vector (19) is orientation dependent, and the volume integral must be evaluated numerically in real time. In order to reduce the computation to a tractable form so that an optimized set of current inputs can be computed and implemented in real-time, it is desired to express the inverse torque model in closed form. It has been shown in [6] that for a spherical motor with linear magnetic properties, the torque generated by the interaction of one stator EM pole pair with  $m_r$  rotor PM pole-pairs can be calculated by summing up its individual interaction with  $m_r$  rotor pole-pairs. Thus, the torque characteristic vector in (19) due to the interaction of one stator pole-air and  $m_r$  rotor pole-pairs can be evaluated as follows:

$$\hat{K}_j (\in \mathbb{R}^{3 \times 1}) = \begin{cases} -\sum_{k=1}^{m_r} \left\{ \hat{f}(\varphi) \begin{bmatrix} \mathbf{s}_j \times \mathbf{r}_k \\ |\mathbf{s}_j \times \mathbf{r}_k| \end{bmatrix} \right\} & \text{if } \mathbf{s}_j \times \mathbf{r}_k \neq 0 \\ 0 & \text{if } \mathbf{s}_j \times \mathbf{r}_k = 0 \end{cases} \quad (20)$$

where  $\hat{f}(\varphi)$  is a curve-fit function derived from (18) as a separation angle  $\varphi$  between a PM pole-pair and an EM pole-pair as shown in Fig. 6(a); and

$$\varphi_{jk} = \cos^{-1} \left[ (\mathbf{s}_j \cdot \mathbf{r}_k) / (|\mathbf{s}_j| |\mathbf{r}_k|) \right].$$

The actual current input vector  $\mathbf{u}$  is found by minimizing the control input energy consumption:

$$J = \frac{1}{2} \mathbf{u}^T [\mathbf{W}] \mathbf{u} \quad (21)$$

subject to the desired torque constraint

$$\mathbf{T}_d = [\hat{K}_1 \cdots \hat{K}_j \cdots \hat{K}_{m_s}] \mathbf{u}$$

where  $[\mathbf{W}] \in \mathbb{R}^{m_s \times m_s}$  is a positive-definite weighting matrix; and  $\hat{K}_j$  is given in closed-form in (20). Provided that the control currents are kept within limits, the optimal  $\mathbf{u}$  can be solved using Lagrange multipliers. The optimal solution can be written in closed form:

$$\mathbf{u} = [\mathbf{K}]^T \left( [\mathbf{K}] [\mathbf{K}]^T \right)^{-1} \mathbf{T}_d \quad (22)$$

In implementation, saturation limits are imposed on the controller to ensure the current inputs are within the amplifier limitations. The eventual stability of the system depends on whether the spherical motor can generate the desired torque.

For completeness, the rotor dynamics is given in the appendix. Using Lyapunov stability analysis, it can be shown that the desired torque for a PD controller can drive the spherical rotor from its initial state to a specified final state:

$$\mathbf{T}_d = [\mathbf{K}_p] \tilde{\mathbf{x}}_1(\mathbf{t}) + [\mathbf{K}_d] \tilde{\mathbf{x}}_2(\mathbf{t}) \quad (23)$$

where  $\tilde{\mathbf{x}}_1(\mathbf{t}) = \mathbf{q}_d - \mathbf{q}(\mathbf{t})$  and  $\tilde{\mathbf{x}}_2(\mathbf{t}) = \dot{\mathbf{q}}_d - \dot{\mathbf{q}}(\mathbf{t})$  define the tracking error and its derivative; and  $\mathbf{q} = [\psi \ \theta \ \phi]^T$  is the orientation vector of Euler angles. For real-time control and motion simulation, the closed-form inverse model (22) is used in real-time control while the full torque model (18) is retained to faithfully predict the motion of the spherical motor.

## IV. SIMULATION AND EXPERIMENTAL RESULTS

We illustrate and validate the DMP model for computing of the magnetic torques by comparing the simulated results against published experimental data and by evaluating the performance between two different designs, Design A (VRSM [6]) and Design B (SWM [14]) in Fig. 3. In both designs, the coils are air cored and other parameters used in the following simulations are given in Table 1:

- A) validation of DMP model for torque computation, and
- B) application of the DMP model to a spherical motor.

Given the specified trajectory, the steps and functional models for a typical feedback cycle (Fig. 3) are as follows:

- 
- Step 1: Compute  $\mathbf{T}_d$  from the inverse dynamics given in Appendix.
  - Step 2: Optimize the control input vector  $\mathbf{u}$  using (23).
  - Step 3: Compute the actual torque  $\mathbf{T}$  from (18), (19) and (22).
  - Step 4: From the rotor dynamics given in Appendix, the actual trajectory of the spherical motor is computed.
  - Step 5: Outputs  $(\alpha, \beta, \gamma)$  are then fed back. Since the focus here is to illustrate the DMP, unity feedback is assumed.
- 

### A. Validation of DMP Model for Torque Computation

The PM's used in both designs have a unity aspect ratio (or  $\gamma = 2a/\ell = 1$ ). Using MATLAB Optimization Toolbox, the parameters,  $k$ ,  $n$ ,  $\delta$ ,  $m_j$  and  $m_o$  were solved for  $\gamma \leq 1$  by minimizing (10) subject to constraints (7) where  $\varepsilon_\theta = 0.05\%$ , (8) and (13). For a PM with constant magnetization, the known field points,  $\Phi = \Phi_a(0, a, \ell/2)$  in (8), can be found numerically from the following expression:

$$\Phi_A = \frac{1}{4\pi} \int_S \frac{\mathbf{M} \cdot \mathbf{n}}{|\mathbf{R} - \mathbf{R}'|} dS$$

Since (10) is singular at the surface, the  $\Phi_A$  values for (10) are solved numerically with  $|\mathbf{R}'| + 10^{-6}$ ; no significant difference in results was found when  $\varepsilon_r \leq 10^{-3}$ . The calculated DMP model for the PM with unity aspect ratio is summarized in Table 2, where the error is defined as

$$\%Error = 100 \times \frac{\int_z |\Phi(z) - \Phi_A(z)| dz}{\int_z |\Phi_A(z)| dz}$$

The simulated fields using the DMP models are compared with the exact solutions in Fig. 4. As expected in (14) and (15), the normalized potential and density field,  $\Phi_A(Z)/(M_o \ell)$  and  $B_A(Z)/(\mu_o M_o)$ , are only a function of the aspect ratio  $\gamma$ . Figure 4 shows that the exact solutions agree well with the field solutions based on only 7 dipoles ( $n=6$  and  $k=1$ ). The discrepancy primarily occurs in the magnetic flux density around the corner; it can be reduced by using more loops (Fig. 5).

To examine the effect of the DMP model on the prediction of magnetic forces, we compute the torque exerted on the EM pole-pairs in the magnetic field of the rotor using (17), where the magnetic flux density is given by (8) along with the DMP model summarized in Table 2.

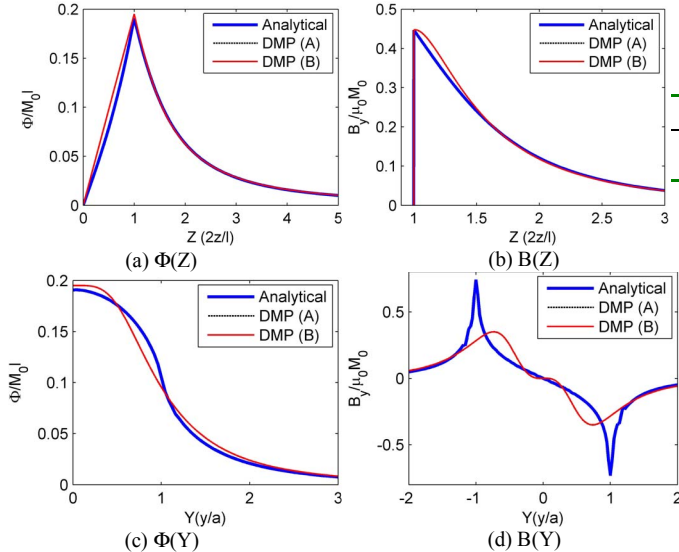


Fig. 4 Potential and flux density along Y and Z axes ( $n=6$  and  $k=1$ )

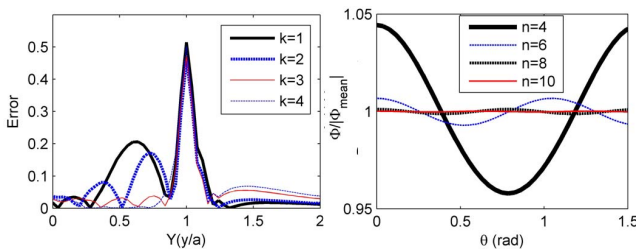


Fig. 5 Effect of  $n$  and  $k$  on modeling errors of PM with  $\gamma(2a/\ell) = 1$

For the purpose of validating the force computation, we simulate the torque for Design A since numerical solutions computed using ANSYS, a commercial finite element (FE) package, are available for comparison [6]. In Case 1, we compute the torque generated by the interaction between the

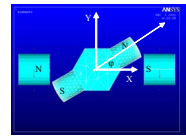
EM pole-pair  $\mathbf{s}_1$  and the PM pole-pair  $\mathbf{r}_1$  as shown in Fig. 6(a), where the pole locations are defined (14) and (15). Case 2 is identical to Case 1 except that the interaction is between  $\mathbf{s}_1$  and  $\mathbf{r}_2$ . Case 3 was performed to determine the principle of superposition holds, which compares the superposition of the two individual cases against the torque calculated with  $\mathbf{s}_1$  and the combined  $\mathbf{r}_1$  and  $\mathbf{r}_2$ . In each of these cases, the stator coils are given a current of 4 Amperes. As shown in Fig. 6(b), the torques computed using the DMP model as a function of rotor position agrees well with the ANSYS results.

Table 1 Rotor Parameters

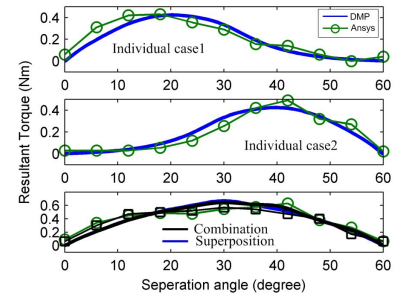
Parameters	Design A [6]	Design B [14]
<b>Rotor</b>		
Rotor diameter, mm(inch)	76.2 (3)	76.2 (3)
PM, number of	6 (1 layer)	16 (2 layers of 8)
Magnetization axis	$\gamma_r = 0^\circ; \delta_r = 60^\circ$	$\gamma_r = 20^\circ; \delta_r = 45^\circ$
$M_o$ , Tesla	1.12	1.35
OD= $2\ell$ mm (inch)	19.05 (0.75)	12.7 (0.5)
Aspect ratio $\gamma(2a/\ell)$	1	1
Moment of inertia (kg-m <sup>2</sup> )	$I_a = 7.00e-4; I_t = 3.50e-5$	$I_a = 6.06e-5; I_t = 3.86e-5$
Offset of mass centre	$\bar{r} = 0$	$\bar{r} = 0$
<b>Stator</b>		
Air-gap, mm(inch)	0.762 (0.03)	0.762 (0.03)
EM, number of	10 (1 layer)	20 (2 layers of 10)
Magnetization axis	$\gamma_s = 26^\circ; \delta_s = 36^\circ$	$\gamma_s = 26^\circ; \delta_s = 36^\circ$
ID/OD/ $2\ell$ mm	9.53/12.7/25.4	9.53/19.05/25.4
Number of coil turns	600	1050
29AWG wire, resist. $\Omega$	6.46	10.51

Table 2 Values of the parameters ( $k=1, n=6$ )

DMP Model	$\delta = \bar{\ell}/\ell$	$m (T/m^2) \times 1.0e-4$	%Error
Design A	0.5141	$m_o = -0.424; m_{t1} = 1.151$	0.998
Design B	0.5136	$m_o = -0.229; m_{t1} = 0.618$	1.00



(a) Torque computation between a PM and an EM pole-pairs



(b) Comparison of torque computation

Fig. 6 Torque Computation using the DMP model

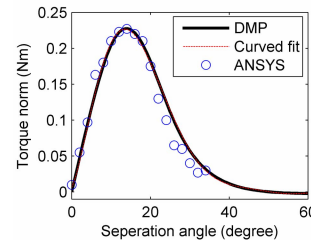


Fig. 7 Torque between a PM pole-pair and an EM pole-pair

7<sup>th</sup> order polynomial fit function:

$$\hat{f}(\varphi) = \sum_{k=0}^7 c_k \varphi^k \quad \text{where } c_0 = -53.18;$$

$$c_1 = 232.51; c_2 = -402.68;$$

$$c_3 = 343.74; c_4 = -142.27; c_5 = 20.61;$$

$$c_6 = 1.25; \text{ and } c_7 = 0.01$$

### B. Application of DMP models in Spherical Motor Control

Once the magnetic field is characterized by the DMP model, the torque model can be computed from (18). Figure 8 graphs the torque between a PM pole-pair and an EM pole-pair as shown in Fig. 6(a) for Design B.

In Fig. 8, the result is compared against those obtained using ANSYS. We note that the accuracy of the ANSYS results depends significantly on the resolution of the mesh. It

addition, the FE analysis must cover a relatively large free space to include the magnetic fields and thus demands significant computational time. Unlike ANSYS results where a few data are available, the torque (18) computed using the DMP model is smooth and can be easily curve-fitted as shown in Fig. 7, where the average error of the 7<sup>th</sup> order polynomial curve-fit is less than 0.02%.

As an illustrative application, we simulate the closed loop control system performance using the torque model computed with the DMP model. The simulation assumes that the orientation measurement system to have no dynamics. For a specified  $\mathbf{T}_d$ , the optimized set of current inputs can be determined from (22) with the curve fit function  $\hat{f}(\varphi)$  given in Fig. 7. With the following PD gains

$$[\mathbf{K}_p] = \begin{bmatrix} 0.5 & 0 & 0 \\ 0 & 0.3 & 0 \\ 0 & 0 & 0.5 \end{bmatrix} \text{ and } [\mathbf{K}_d] = 0.5\mathbf{I}$$

where  $\mathbf{I}$  is 3x3 identity matrix, the simulation results for a step change in rotor orientation from its initial upright position ( $\alpha = \beta = \gamma = 0^\circ$ ) to the final state ( $\alpha = 0^\circ$ ,  $\beta = 10^\circ$  and  $\gamma = 60^\circ$ ) are given in Fig. 8.

To examine the effect of the curve-fit function based on the DMP model, we compare the full model (19) and the simplified closed-form solution (20) in modeling the forward torque. As shown in Fig. 8 and Table 3, the comparisons show very good agreement with less than 15% error in both the computed torque and the simulated motions.

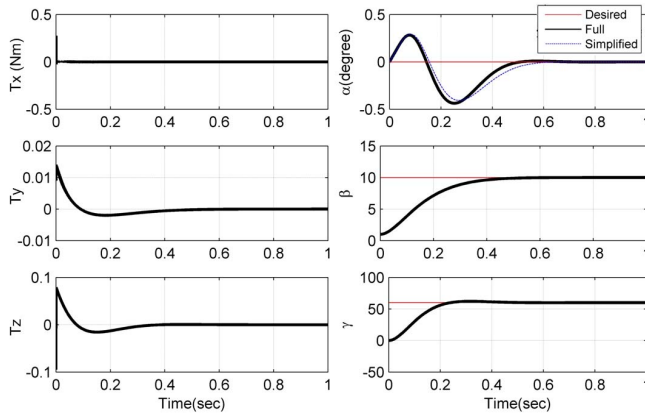


Fig. 8 Step response of Spherical Motor (Design B)

Table 3 Maximum percentage error

Torques (%)			Angles (%)		
$T_x$	$T_y$	$T_z$	$\alpha$	$\beta$	$\gamma$
9.78	4.37	6.02	13.9	7.6	10.4

## V. CONCLUSIONS

A new model providing a means to derive closed-form field solutions and magnetic torques of a PM-based spherical motor has been presented. This method extends the concept of a magnetic doublet beyond the context of physics, but accounts for the shape and magnetization of a physical PM. The modeling method has been validated by comparing the computational results against published experimental and numerical data. The simplicity of the closed-form solutions along with precise (and yet intuitive) magnetic fields of the DMP models have been demonstrated with practical examples of torque modeling and motion simulation.

## REFERENCES

- [1] Clarke, W., "Mercedes-Benz F-400 Carving," edmunds.com, 2002
- [2] Peter, J., "The Wave of the Future?" *Automotive Industries*, Jan. 2004
- [3] Lee, K.-M. and C. Kwan, "Design concept development of a spherical stepper for robotic applications", *IEEE Trans. on Robotics and Automation*, Feb. 1991. 7(1), pp 175-181.
- [4] Wang, J., G. Jewell, and D. Howe, "Design and control of a novel spherical permanent magnet actuator with three degrees of freedom", *IEEE/ASME Trans. on Mechatronics*, Dec.2003. 8(4), pp. 457.
- [5] Liang, Y., I. M. Chen, G. Yang, L. Wei, and K.-M. Lee, "Analytical and experimental Investigation on the Magnetic Field and torque of a Permanent Magnet Spherical Actuator," *IEEE/ASME Trans. on Mechatronics*, Aug. 2006. 11(4), pp. 409-419.
- [6] Lee, K.-M. R. A. Sosseh and Z. Wei, "Effects of the Torque Model on the Control of a VR Spherical Motor," *IFAC Journal of Control Engineering Practice*, Nov. 2004. 12(11), pp 1437-1449.
- [7] Li, Qiang and K.-M. Lee, "An adaptive meshless computation method for design of electromechanical actuators," *IEEE Trans. on Magnetics*, Aug. 2006. 42(8), pp. 1996-2002.
- [8] Craik, D. J., "Magnetostatics of axially symmetric structure", *J. of Physics*, 1974. 7, pp. 1566.
- [9] Green, M. A., "Modeling the behavior of oriented permanent magnet material using current doublet theory", *IEEE Trans. on Magnetics*, Mar. 1988. 24(2) pp. 1528.
- [10] Bennett, W. S., "Basic sources of electric and magnetic fields newly examined", *IEEE Antennas and Propagation Magazine*, Feb. 2001. 43(1) pp. 31-5.
- [11] Nedelcu, S. and J. H. P. Watson, "Magnetic dipole model of a permanent magnet based device", *J. of Physics*, Sep. 2001. 34(17) pp. 2622-2628.
- [12] Visschere, D. and R. Patrick, "An exact two-dimensional model for a periodic circular array of head-to-head permanent magnets", *J. of Physics D: Applied Physics*, Feb. 2005. 38(3) pp. 355-362.
- [13] Jackson, J.D. "Classical electrodynamics" New York : Wiley, 1999
- [14] Lee, K.-M. and H. Son. "Torque model for design and control of a spherical wheel motor", *IEEE/ASME AIM2005 Proc.* Jul. 2005. 1, pp. 335-340

## APPENDIX: EQUATIONS OF ROTOR MOTION

The motion of SWM can be characterized in term of ZYZ Euler angles ( $\alpha$ ,  $\beta$ ,  $\gamma$ ). For the mechanical structure, the equation of rotor motion derived using the Lagrangian formulation has the following form:

$$[\mathbf{M}] \ddot{\mathbf{q}} + \mathbf{C}(\dot{\mathbf{q}}, \mathbf{q}) = \mathbf{Q} \quad (\text{A.1})$$

where

$$[\mathbf{M}] = \begin{bmatrix} (I_a - I_t) \cos^2 \beta + I_t & 0 & I_a \cos \beta \\ 0 & I_t & 0 \\ I_a \cos \beta & 0 & I_a \end{bmatrix} \quad (\text{A.2})$$

$$\mathbf{C}(\dot{\mathbf{q}}, \mathbf{q}) = \begin{bmatrix} 2(I_t - I_a) \sin \beta \cos \beta \dot{\alpha} \dot{\beta} - I_a \sin \beta \dot{\beta} \dot{\gamma} \\ (I_a - I_t) \sin \beta \cos \beta \dot{\alpha}^2 + I_a \sin \beta \dot{\alpha} \dot{\gamma} \\ -I_a \sin \beta \dot{\alpha} \dot{\beta} \end{bmatrix} \quad (\text{A.3})$$

and

$$\mathbf{Q} = \begin{bmatrix} -T_1 \sin \beta \cos \gamma + T_2 \sin \beta \sin \gamma + T_3 \cos \beta \\ mgh \sin \beta + T_1 \sin \gamma + T_2 \cos \gamma \\ T_3 \end{bmatrix} \quad (\text{A.4})$$

where  $\mathbf{q} = [\alpha \beta \gamma]^T$ ;  $I_a = I_{zz}$ ;  $I_t = I_{xx} = I_{yy}$ ; and  $m$  is the mass of the rotor.

In (A.3),  $h$  accounts for the off-center of the mass; and  $\mathbf{Q}$  represents the contributions of the applied torque to the generalized moments. The applied torque in the rotor frame is expressed by the stator frame as

$$\mathbf{T}_{123} = [\Gamma] \mathbf{T}_{XYZ} \quad (\text{A.5})$$

where

$$\mathbf{T}_{123}^T = [T_1 \ T_2 \ T_3]; \quad \mathbf{T}_{123}^T = [T_1 \ T_2 \ T_3]; \quad \text{and}$$

$$[\Gamma] = \begin{bmatrix} \cos \alpha \cos \beta \cos \gamma - \sin \alpha \sin \gamma & \sin \alpha \cos \beta \sin \gamma + \cos \psi \sin \gamma & \sin \beta \cos \gamma \\ -\cos \alpha \cos \beta \sin \gamma - \sin \alpha \cos \gamma & -\sin \alpha \cos \beta \sin \gamma + \cos \psi \cos \gamma & \sin \beta \sin \gamma \\ \cos \alpha \sin \beta & \sin \alpha \sin \beta & \cos \beta \end{bmatrix}$$